Mining, Metallurgy & Exploration (2019) 36:235–244
https://doi.org/10.1007/s42461-018-0035-5

Selective Extraction of Rare Earth Elements from Monazite Ores with High Iron Content

Leandro Augusto Viana Teixeira[1,2] · Ruberlan Gomes Silva[1] · Angela Avelar[1] · Daniel Majuste[2,3] · Virginia S. T. Ciminelli[2,3]

Received: 27 September 2018 / Accepted: 12 December 2018 / Published online: 4 January 2019

Abstract

Rare earth elements are essential for modern life products and green technologies. Recent supply constraints have boosted the development of rare earth projects after the price peak of 2011. The feasibility of a project depends on the definition of a processing route, which in turn depends primarily on the rare earth mineral, with monazite and bastnaesite representing the two most relevant minerals. Monazite-type ores usually contain high acid consumption impurities, such as iron, aluminum, calcium, magnesium, and phosphates, and may also contain prohibitive levels of radioactive thorium in its composition. This work presents a thermodynamic analysis of a monazite system and discusses the fundamentals of a selective process route for rare earth extraction from monazite ores with high iron content. This process involves sulfation by means of concentrated sulfuric acid and roasting at a high temperature. The route yields high rare earth extraction with low iron and thorium extractions and low acid consumption. Rare earth extractions as high as 80% were achieved, while iron and thorium extractions were lower than 1%, and acid consumption was lower than 0.34 kg of sulfuric acid per kg of ore. The operational window was compared to the one predicted by thermodynamic modeling, with 700 °C representing the optimal roasting temperature.

Keywords Rare earth extraction · Monazite ore · Sulfuric acid · Selective roasting

1 Introduction

Rare earth elements (REE) can be defined as the 15 elements of the lanthanide series (ranging from lanthanum to lutetium) plus yttrium and scandium. Although yttrium and scandium do not belong to the lanthanide series, they are treated as rare earth elements due to their similar chemical behavior and natural co-occurrence with the other 15 elements. Main drivers for rare earth consumption are the catalysts, magnets, polishing powders, and rechargeable battery electrodes. Other relevant applications are in the metallurgical, ceramics, phosphors and pigments, and glass industry [1].

Rare earths are widely spread in low concentrations throughout the earth's crust. They are found in more than 160 discrete minerals, but 95% of all the world's rare earth resources occur in just four minerals: bastnaesite (Ce, La, Y) (CO_3) F, monazite (Ce, La, Pr, Nd, Th, Y) PO_4, xenotime (YPO_4), and ion-adsorption clays. Bastnaesite and monazite are minerals rich in light rare earth elements (LREE), whereas xenotime and ion-adsorption clays are rich in high rare earth elements (HREE). The rare earth content in deposits is usually low, seldom higher than 5% *w*/*w* [2], and it is usually extracted as a by-product or a co-product [3]. Monazite and bastnaesite account for most of the REE available in the world. Figure 1 illustrates the large rare earth deposits in China, Brazil, Vietnam, Namibia, Russia, India, and Australia. The relevance of monazite as one of the main rare earth carriers is also highlighted. Most of the current rare earth production comes from China, Bayon Obo being the largest operation. Outside China, Mountain Pass (USA) and Mount Weld (Australia) are worth mentioning due to their relevance and production capacity. Mount Pass used to process typical bastnaesite

✉ Virginia S. T. Ciminelli
ciminelli@demet.ufmg.br

Leandro Augusto Viana Teixeira
leandro.viana.teixeira@vale.com

[1] Vale Mineral Development Centre, Rodovia BR 381, km 450, Distrito Industrial Simão da Cunha, Santa Luzia, MG 33040-900, Brazil

[2] Universidade Federal de Minas Gerais, Av. Presidente Antônio Carlos, 6677, Belo Horizonte 31270901, Brazil

[3] National Institute of Science and Technology on Minerals Resources, Water and Biodiversity, INCT-Acqua, Belo Horizonte, Brazil

ore, whereas Mountain Weld extracts monazite ore and ships it to Malaysia, where it is processed. Bayan Obo, in China, operates with a mix of bastnaesite and monazite.

Since the 1990s, China has become the largest REE producer and exporter in the world. In 2010, this country was responsible for 92% of the world's total production. In the same year, China reduced the exportation quotas by 22.5%, leading to a shortage worldwide and to a very high spike in prices, reaching its maximum values in 2011. This spike in prices stimulated the discovery of new deposits and the development of hundreds of mineral projects around the world. It also resulted in very intensive technological research with the aim of developing new alternatives for rare earth processing and separation. The prices started to fall in 2015 and are now at the level they were before the implementation of the quota system, except for neodymium and praseodymium, which are still displaying high price levels due to green technology development. Figure 2 shows the price change for some rare earth oxides (REO) since 2004. As the technologies take time to mature, some outcomes of the technology rush are now being presented to the world. Most of the projects created during the price spike of 2011 are currently on hold, waiting for better prices.

This work focuses on the need for a processing route that can extract rare earth elements from complex ores. The term complex ores means, in this context, ores that show poor performance under conventional mineral beneficiation (e.g., flotation and gravity concentration) due to very fine, micro-level association between the main REE carrying mineral (monazite) and the gangue material. This type of ore does not allow relevant REE upgrades prior to the hydrometallurgical processing and, within its composition, may also carry acid-consuming elements and impurities (e.g., Fe, Mg, Th, U, and F) that will bring technical difficulties and negative economic impacts to the project. An efficient extraction process should minimize the impurities carried to downstream steps and keep acid consumption as low as possible. The selective roasting, as discussed here, allows for the separation of iron and thorium from the rare earth elements, significantly decreasing the impurity levels in the liquor obtained by water leaching.

The experimental results will demonstrate the selective extraction of rare earth elements, particularly with respect to iron and thorium. The effect of the roasting temperature and time on the selective extraction will be presented, as well as the decomposition behavior of sulfates during roasting by means of mass loss. A thermodynamic evaluation of the proposed process, including both the sulfation and roasting stages, will also be reported.

2 REE Extraction from Monazite Ores

Rare earth extraction usually involves a physical beneficiation and a hydrometallurgical process. A pyrometallurgical step may also be required to prepare the ore for the hydrometallurgical stage. The physical beneficiation produces the concentrate (almost no market outside China), whereas the pyro and hydrometallurgical processing of the concentrate produces a mixed rare earth material (restricted market). This material must comply with market specifications in order to proceed to the separation stage. Several steps of liquor purification are added to the flowsheet to attain this specification. The mixed material is then fed in the separation plants (these plants usually operate large solvent extraction facilities) to produce the separated rare earth elements. The rare earth compounds,

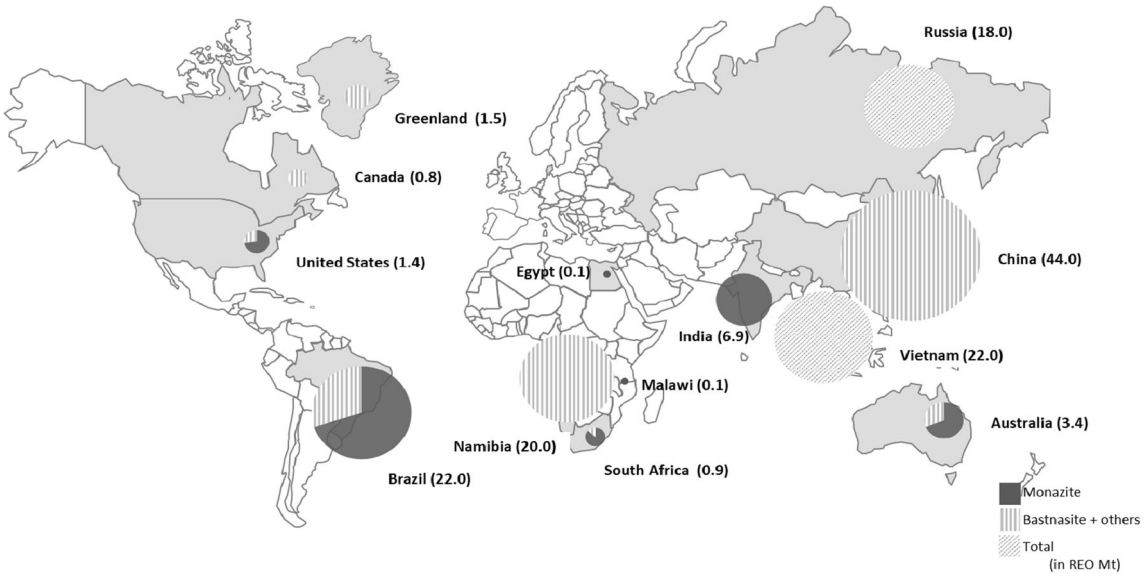

Fig. 1 Estimated global rare earth resources and its distribution between monazite and bastnaesite. Total represents unspecified mineral resources. Based on data from [3, 4]

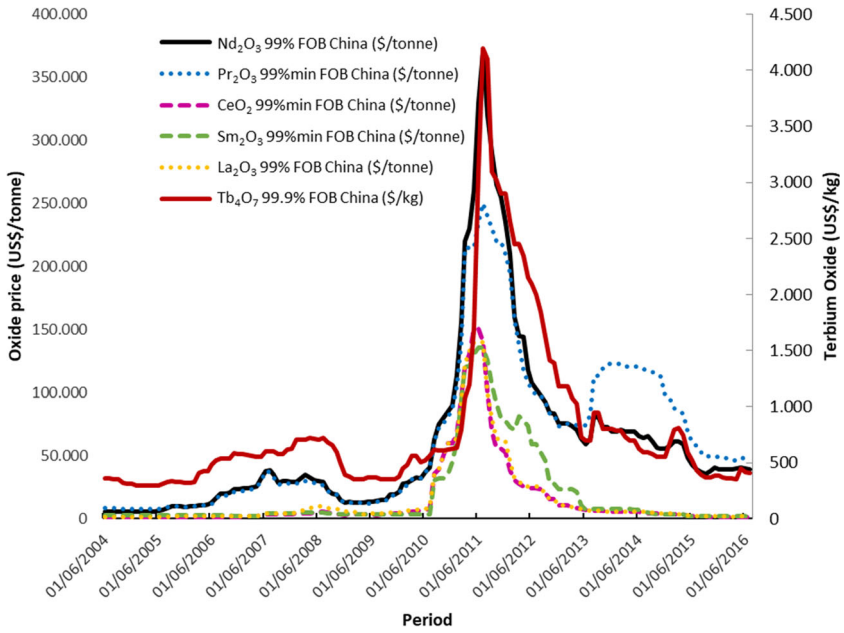

Fig. 2 Price change for rare earth oxides of praseodymium, neodymium, cerium, samarium lanthanum (to the left), and terbium (to the right). Based on data from [5]

usually oxides, carbonates, chlorides, among others, are sold to their final application or may be even further processed to increase purity level or to be turned into a different compound (e.g., metallic form in alloy) [3].

The beneficiation and chemical extraction of rare earths depend strongly on the mineral carrier. The physical beneficiation of monazite ores is usually difficult due to high weathering profiles of the deposits. Beneficiation may involve gravity concentration or magnetic/electrostatic separation. Flotation may be applied in a few cases, as it is better established for bastnaesite and is present in most industrial circuits that treat this type of ore [3, 6].

Due to its wide variation in chemical composition and weathering profile, monazite has a wider range of processing options than does bastnaesite. The treatment of monazite ores is usually divided into two main groups—the hydroxide and sulfuric acid processes—the latter of which is of interest in the present investigation.

The standard sulfuric acid process of monazite consists of (i) acid addition to the ore (the ratio acid/ore may vary widely), followed by (ii) heating in order to increase the conversion of rare earth phosphates to rare earth sulfates, (iii) dissolution in water [1], and (iv) purification to obtain a rare earth compound (such as hydroxide, oxalate, chloride, or carbonate). The selection of the acid/ore mass ratio (usually between 1/1 and 2/1 [7]) is very important, since it has a direct impact on the process' economic performance and amount and type of impurity that will be carried downstream. The acid-ore mixture is usually heated in a rotary kiln under temperatures ranging from 200 to 600 °C to enhance the sulfation reaction. The higher the acid to ore ratio, the higher the dissolution of impurities during leaching. The heating stage can be divided into low temperature (below 300 °C) and high temperature (above 300 °C) [7]. Sulfates generated during the sulfation and the heating stages (Eqs. (1) and (2)) will dissolve during water leaching, generating a rich-liquor in rare earth but also containing several impurities. After leaching, the rare earths are then precipitated as double sulfates, which in turn are converted to hydroxides, dried, and leached with nitric acid to remove Th and Ce. Rare earths in the liquor are re-precipitated as mixed hydroxides and sent to the separation plants. The low-temperature process is older and renders a complex solution after leaching, making it more difficult to remove impurities. The high-temperature process decreases thorium extraction due to the formation of insoluble ThP_2O_7 [7].

$$2(\mathrm{REE})\mathrm{PO}_{4(s)} + 3\mathrm{H}_2\mathrm{SO}_{4(aq)} \rightarrow 2\mathrm{H}_3\mathrm{PO}_{4(aq)} + (\mathrm{REE})_2(\mathrm{SO}_4)_{3(s)} \quad (1)$$

$$\mathrm{Th}_3(\mathrm{PO}_4)_{4(s)} + 6\mathrm{H}_2\mathrm{SO}_{4(aq)} \rightarrow 4\mathrm{H}_3\mathrm{PO}_{4(aq)} + 3\mathrm{Th}(\mathrm{SO}_4)_{2(s)} \quad (2)$$

The previously described process routes are the standard flowsheets for rare earth processing. Modifications are required to address specific characteristics of the ore, such as high iron content. There are several modifications of the standard processes as an attempt to reduce impurity dissolution and acid consumption, as well as to increase rare earth extraction. A summary of some modifications of the standard process for REE extraction is show on Table 1. Those modifications can be divided into two groups. One group [11, 12] attempted to use another type of mineral acid to improve REE extraction. Another group [8–10, 13–15] attempted to

Table 1 Relevant process modifications for REE extraction of monazite ores using sulfation/leaching/roasting techniques

Author	Year	Ore	Extraction type	Acid	Heating
Merrit [8]	1990	Monazite	Leaching	HCl	977–1187 °C
Reneau and Tognet [9]	2003	Monazite	Sulfation	H_2SO_4	780 °C
Huang et al. [10]	2009	Monazite	Leaching	H_2SO_4	231–600 °C
Mackowski et al. [11]	2009	Monazite Apatite	Sulfation Leaching	$HCl/HNO_3/H_2SO_4$	230 °C
Boudreault et al. [12]	2012	Several	Leaching	$HCl/HNO_3/H_2SO_4$	80–225 °C
Berni et al. [13]	2013	Monazite	Sulfation Leaching	H_2SO_4	400–800 °C
Teixeira and Silva [14]	2014	Monazite Tailings Industrial residue	Sulfation Leaching	H_2SO_4	Optional (650–750 °C)
Onal et al. [15]	2015	Scrap	Sulfation Leaching	H_2SO_4	750–800 °C

use different reagents or process conditions to promote a selective extraction of rare earths. These processes may have the aim of separating thorium as an insoluble compound [8, 13, 14] or minimizing extraction due to temperature-related formation of insoluble compounds.

Berni [13] presented a process route in which iron is separated from rare earth in monazite ores by using a sulfation stage followed by selective roasting. This process was modified by the author [14] by introducing intensive mixing, which allowed direct leaching in water, yielding a large rare earth extraction ratio even without roasting. A roasting stage may take place at 700 °C to decompose iron sulfate into iron oxide, the latter being insoluble at pH higher than two, and the sulfur trioxide released can be recovered and reused in the process. In 2015, Onal [15] presented a similar process for Nd recovery from FeBNd scrap, where selective roasting is applied between 650 and 750 °C. Verbaan [16] reviewed 18 concentrate leaching projects and noticed that 11 of these used sulfuric acid as a primary lixiviant. Among these projects, seven are using roasting as part of the flowsheet. The authors state that, although sulfuric acid roasting is considered a mature technology in China, it is not a common processing technology in the Western World.

As mentioned in the previous paragraphs, there are several process routes for monazite processing, but none of them are clear with regard to their mechanisms or industrial advantages. The process described by Berni [13] and further developed by Teixeira and Silva [14] shows the possibility of rare earth extraction with low acid consumption and low impurity loading into the leaching solution, but the mechanisms behind this process are still unclear. Thus, the objective of the present investigation is to provide a thermodynamic background for the selective roasting method and apply such a technique to complex, iron-rich, monazite ores. The behavior of rare earth, thorium, and iron during this process is also discussed.

3 Experimental Procedure

3.1 Materials

Reagent-grade ferric sulfate ($Fe_2(SO_4)_3 \cdot xH_2O$, Fe 22.0% min), 97.5% *w*/*w* sulfuric acid (Anidrol), 99.9% lanthanum sulfate (Fmaia, $La_2O_3/REO > 99.99\%$), and natural fines (< 74 μm) of a monazite ore from a phosphate mine were used in the experiments.

3.2 Rare Earth Extraction

The extraction experiments were comprised of the following steps: (i) separation of natural fines (< 74 μm) by scrubbing a 50% *w*/*w* suspended solid ore pulp for 15 min and passing this material through a 74 μm sieve [17]; (ii) sulfation by mixing the natural fines (200 g minimum) with sulfuric acid 97.5% *w*/*w* for 30 min using a 1.5-L mechanical mixer (Marconi, model MA259); (iii) roasting in a muffle-type furnace (K-type thermocouple) under air for 2 h; (iv) cooling the charge to 20 °C; and (v) leaching the solids in water at 10% *w*/*w* for 2 h at room temperature, under mechanical mixing (200–300 rpm). The pH was controlled (when necessary) between 1.5 and 2.0 by adding sulfuric acid (Mettler Toledo pH meter type M400). The REE extraction was performed following the procedure described by Teixeira and Silva [14] and Berni [13]. The amount of acid added to each sample changed based on its composition, ranging from 0.21 to 0.34 kg of acid per kg of sample. Roasting temperature ranged from 200 to 800 °C.

3.3 Analytical Methods

The TGA-DTA analyses were performed in a Netzsch STA 449F3 equipment, under synthetic air atmosphere in an alumina crucible with a heating rate of 10 K min^{-1} up to 1000 °C (1400 °C for $La_2(SO_4)_3$).

Solid and aqueous solutions were analyzed by Inductively Coupled Plasma Optical Emission Spectrometry-ICP-OES (Varian, VISTA PRO model) and Inductively Coupled Plasma Mass Spectrometry (PerkinElmer ICP-MS, model NexION 300D). Duplicates, blanks, and standards (DBS) were used during ICP analysis. Samples were subjected to an acceptable duplicate maximum mean error (ME) that varied with the method, the element, and concentration. Prior to chemical analyses, solid samples were dried in an oven at 100 °C for at least 1 h and pulverized to a condition in which 95% of the particles (in mass) were below 74 μm. The solid samples containing rare earth elements, thorium and uranium (DBS every 24 samples, ME between 10 and 5%) were treated by fusion with $Li_2B_4O_7$ or with H_2O_2 followed by dissolution in 10% (*v*/*v*) nitric acid (65% *v*/*v*). For the analyses of the remaining elements (DBS every 20 samples, ME between 10 and 5%), the samples were treated by fusion with Na_2CO_3 and $Na_2B_4O_7$, followed by dissolution in 67% (v/v) hydrochloric acid. The concentrations of aluminum, iron, phosphorous, sulfur, and the rare earths (Pr, Nd, and Sm) in the solids (after fusion/dissolution) and in aqueous solution after leaching were analyzed by ICP-OES (DBS every 20 samples, ME between 10 and 5%). The concentration of the remaining rare earth elements and other impurities (both from solid samples and leach solutions) were analyzed by ICP-MS, after dilution in 2% *v*/*v* nitric acid (65% *v*/*v*). Rare earth analysis from leach solutions had DBS analyzed every 20 samples and ME between 10 and 5%. The ferrous iron concentration in the leach solution was measured by straight titration with $K_2Cr_2O_7$ in acid solution using barium diphenylamine sulfonate as an indicator.

Samples for X-ray diffraction analysis (XRD) were ground below 74 μm (200 Mesh Tyler) and analyzed on PANalytical Model X'PERT PRO MPD (PW 3419) equipped with a PW3050/60 (θ/θ) goniometer, X-ray ceramics tubes, Co anode (Kα1 = 1.78897 Å), and a PW3373/00 model detector (2000 W-60 kV). The diffraction patterns were acquired from 4 to 78° (2θ) at 0.02 steps. The identification of all minerals was done with X'PertHighScore version 2.1b software from PANalytical by using ICDD (International Center for Diffraction Data) files as a reference (2003 database).

Mineralogical characterization, modal composition, and mineralogical association were performed by XRD analysis, SEM, and QEMSCAN (Quantitative Evaluation of Minerals by scanning electron microscopy) analysis for fraction below 74 μm. Polished sections were made for QEMSCAN and SEM analysis. The chemical results obtained for the given particle sizes were used for data reconciliation.

3.4 Thermodynamic Evaluation

HSC chemistry (Outotec) version 8 [18] provided the thermodynamic data (values for standard enthalpy, entropy, and Gibbs Free energy) and software to generate the stability diagrams.

4 Results and Discussion

4.1 Samples Characterization

The chemical assays of the samples and the respective mineralogy are shown in Table 2 and Fig. 3. The REO content of the samples is similar and falls within the range of 4–5% wt. The ore is rich in iron, with an Fe_2O_3 content of above 30% *w*/*w* in all samples, making iron the most abundant element. In the present work, light rare earth oxides (LREO) include elements from La to Nd, and heavy rare earth oxide (HREO) elements ranging from Pm to Lu, including Y and Sc; Gd was not analyzed due to Pr (141) interference. This definition is broadly accepted and better describes the samples. The LREO/REO ratio is similar in all samples (app. 96%).

Brod et al. [19] defined the bebedourites as being comprised of diopside, phlogopite, magnetite, apatite, and perovskite, interpreted as the partially preserved portion of the intense phlogopitization undergone by the rocks of the complex. Foscorite are rocks composed of magnetite, apatite $(Ca_5(PO_4)_3(F, Cl, OH)$, and olivine $(Mg, Fe)_2SiO_4$, which is present as independent magmatic events, like veins or plugs cracking through silicate and carbonatite rocks in several directions. Ribeiro [20] classified flogopitite as carbon-hydrothermal products derived from the bebedourite series. The lithotype definition is related to the unaltered rock. The samples of this study underwent transformation by weathering, resulting in a different mineralogy when compared to the lithotype definition.

The samples used in this work were collected at the isalterite/aloterite level, which is marked by the disappearance of the phyllosilicates on a macroscopic scale. From this stage, the predominance of iron oxides/hydroxides, clays, phosphates (primary and secondary), and minerals of supergenic alteration (anatase for example) can be observed.

Table 2 Chemical composition of the selected samples

	Bebedourite	Flogopitite	Foscorite
Al (%)	2.96	3.16	2.80
Ba (%)	0.36	1.21	1.28
Ti (%)	12.34	7.53	9.88
Ca (%)	< 0.681	3.84	1.58
Fe (%)	25.79	21.81	24.05
Mg (%)	0.27	2.91	0.96
Mn (%)	0.64	0.78	0.77
P (%)	1.75	3.26	2.72
Si (%)	8.88	9.11	8.15
U (mg kg^{-1})	46	45	50
Th (mg kg^{-1})	352	181	233
REO (%)	4.26	4.70	4.86
LREO/REO	96%	97%	96%

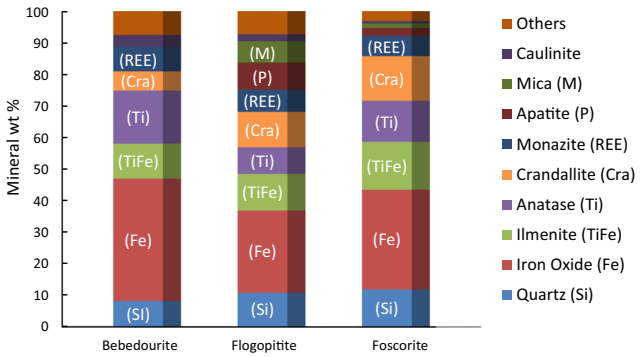

Fig. 3 Mineral composition diagram for bebedourite, flogopitite, and foscorite samples (natural fines < 74 μm)

The main REE carrier is monazite, but near to 5% *w*/*w* of REE is present in candrallite. This partition was estimated by Energy Dispersive Spectroscopy (EDS) analysis and should be further investigated by an EPMA (Electron Probe Micro-Analyzer). Iron is mainly present as iron oxide/hydroxide and ilmenite (Fig. 3).

4.2 Thermodynamic Analysis

In 1973, Bainbridge [21] reported the possibility of achieving selective nickel extraction by gas sulfation, exploiting the difference in sulfate stability between iron and nickel. The same approach can be applied to iron-rich, rare earth ores. The stability of selected rare earth sulfates, iron sulfate, and other metal sulfates with respect to their oxides at the temperature range of 500–1000 °C are shown in Fig. 4. Sulfates formed by reactions at the top of this figure are less stable than those that appear at the bottom, with calcium being the most stable sulfate and aluminum the least stable. The results show a significant difference between the stability of iron and rare earth sulfates, particularly for cerium and lanthanum. The standard Gibbs free energy of formation of iron and aluminum sulfate becomes positive for temperatures over 800 °C, while this property remains negative for the rare earth elements. This implies that the decomposition of iron and aluminum sulfate to their respective oxides (reverse reaction) may take place at higher temperatures, while the sulfates of rare earth elements will remain stable. Among the rare earth elements analyzed here, lanthanum sulfate is the most stable compound and neodymium the least stable.

The thermal stability of different sulfates may also be discussed based on a thermal stability diagram, as shown in Fig. 5. The diagram shows the stability of sulfates according to Eq. (3), where REE represents the rare earth elements and the Delta symbol (Δ) indicates that heat is being added to the system.

$$\mathrm{REE_2(SO_4)_{3(s)}} \rightarrow^{\Delta} \mathrm{REE_2O_{3(s)}} + 3\mathrm{SO_{3(g)}} \quad (3)$$

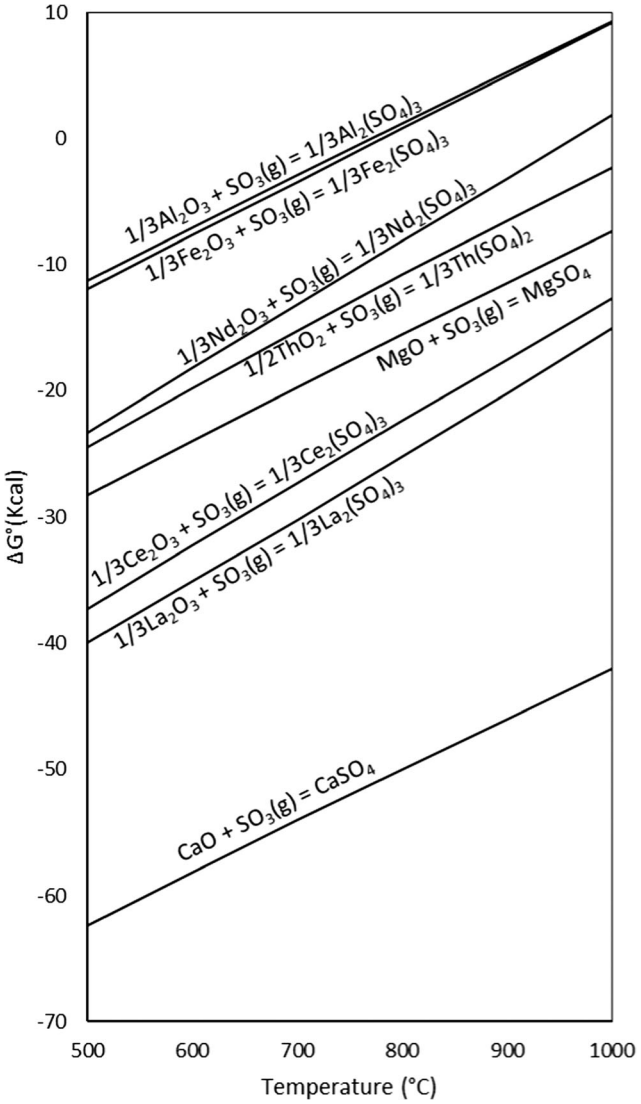

Fig. 4 Variation of the standard Gibbs free energy for the sulfation reaction for different oxides in the temperature range 500–1000 °C (HSC v.8)

The sulfation process proposed in this paper is expected to yield anhydrous sulfates, since no additional water is added during sulfation (the process occurs with only 2.5% wt. water contained in the concentrated sulfuric acid). The sulfation reaction itself is highly exothermic, thus driving off any water remaining in the ore. This is a favorable condition for the formation of anhydrous sulfates, and the presence of hydrated sulfates is unlikely. Nevertheless, the thermodynamic information for Dy, Y, Pr, and Sm were available only as hydrated sulfates and, therefore, these species were kept in the diagram for comparison purposes only. The diagram shows a significant temperature difference between the decomposition of iron sulfate and anhydrous rare earth sulfates: about 150 °C for neodymium (750 °C ➔ 900 °C) and even higher for lanthanum (750 °C ➔ 1100 °C). These findings support the use

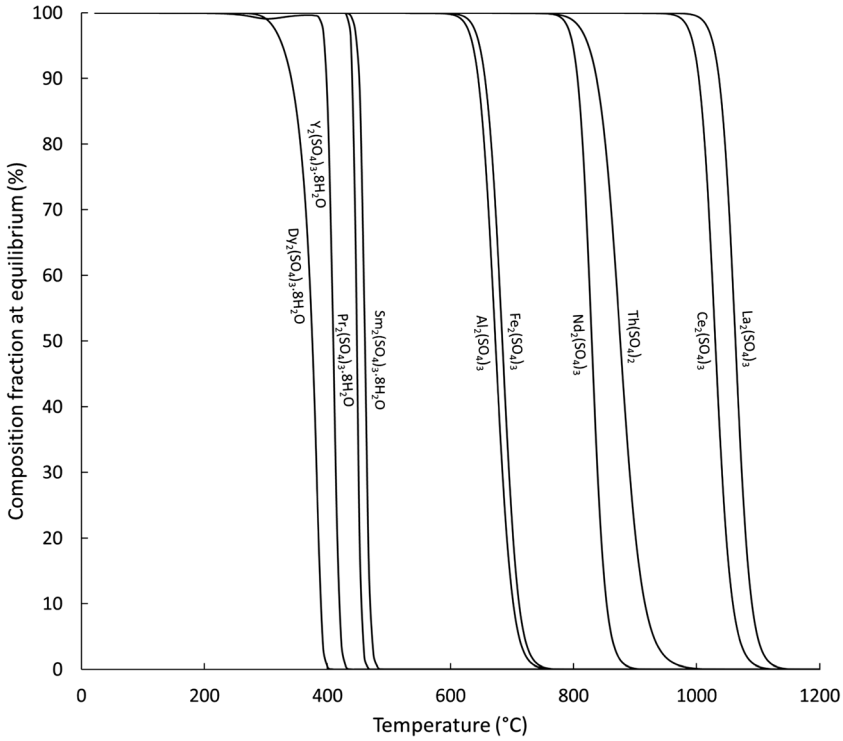

Fig. 5 Thermal stability for some rare earth sulfates and the main impurities present in the ore. The decrease in the fraction of the sulfate compound implies the proportional formation of the respective oxide

of selective roasting at temperatures over 750 °C and under 900 °C (to avoid neodymium sulfate decomposition). Temperatures between 750 and 900 °C would allow for the decomposition of iron sulfate and the formation of iron oxide while keeping most rare earth elements as soluble sulfates. Iron sulfate is soluble in water whereas ferric oxi-hydroxides are insoluble at pH higher than approximately 2. This approach would allow for a high extraction of rare earth elements and a low extraction of iron from a sulfated sample submitted to selective roasting. Following the diagram, hydrated sulfates of Dy, Y, Pr, and Sm would also decompose into oxides, yielding low extraction values for these elements.

4.3 TGA Analysis

To confirm the thermodynamic simulation, the decomposition of ferric sulfate and lanthanum sulfate was investigated by TGA analysis. The results are shown in Fig. 6, including the result obtained for a sulfated (after mixing with sulfuric acid) foscorite sample. A very good agreement was observed between the simulated thermal behavior of the sulfates with the result obtained from the TGA analysis. Although not represented in Fig. 6, the dehydration temperature for lanthanum sulfate took place at temperatures lower than 300 °C, which is in agreement with other reports [22]; however, two points of disagreement may be pointed out: the temperature of dehydration of ferric sulfate and the decomposition pattern of lanthanum sulfate. The hydrated ferric sulfate loses its water molecules at temperatures below 250 °C, but the simulated TGA shows temperatures of about 400 °C. Although 150 °C seems to be a considerable temperature difference, it is not relevant since the formation of hydrated sulfates in this system is unlikely to happen, as discussed before. The simulated system considered the dehydration of $Fe_2(SO_4)_3 \cdot 9H_2O$ directly into an anhydrous ferric sulfate. The real process may take place following successive water loss, hence giving results like that obtained for the $Fe_2(SO_4)_3 \cdot 7H_2O$ sample. The difference in the decomposition pattern of lanthanum sulfate is more relevant. The TGA result shows a two-step decomposition under a synthetic air atmosphere. The first step shows a mass loss of about 27%, while the expected total mass loss for complete sulfate decomposition is about 42%. This intermediary mass loss may indicate partial decomposition of lanthanum sulfate to oxysulfate, $La_2O_2SO_4$ [23, 24].

By using the same technique, Poston [25] reported different decomposition temperatures, with lanthanum sulfate decomposition starting at 775 °C. This difference was likely due to the different atmosphere applied during the TGA analysis. Oxidative atmospheres lead to higher decomposition temperature (1100 °C), inert atmosphere to intermediate temperatures (775 °C), and reductive atmosphere to low temperatures (610 °C) [26].

The foscorite sample is a complex assemblage of several compounds (Fig. 3) and thus displays a mass loss during the entire temperature range of the experiment (Fig. 6); however, it is possible to observe a sharp mass loss at 700 °C, in good agreement with the simulated and the experimental decomposition temperature found from TGA for ferric sulfate

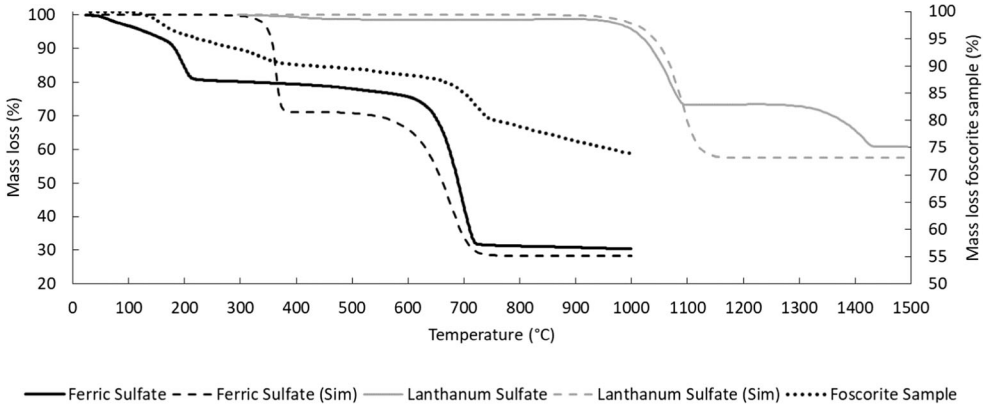

Fig. 6 TGA results for hydrated ferric sulfate ($Fe_2(SO_4)_3 \cdot 9H_2O$) and anhydrous lanthanum sulfate under synthetic air atmosphere and 10 K min^{-1}. The dotted lines are simulations based on HSC thermodynamic data. The mass loss attributable to crystallization water in the lanthanum sulfate was removed to simulate the behavior of anhydrous lanthanum sulfate

decomposition to ferric oxide. The decomposition of trivalent rare earth elements and impurities like ferric sulfate can be described by Eqs. (4), (5), and (6). The existence and amount of SO_3 in the gas phase is defined by the equilibrium constant at a given temperature (Eq. (7)).

$$REE_2(SO_4)_{3(s)} \rightarrow^{\Delta} REE_2O_2SO_{4(s)} + 2SO_{2(g)} + O_{2(g)} \quad (4)$$

$$REE_2O_2SO_{4(s)} \rightarrow^{\Delta} REE_2O_{3(s)} + SO_{2(g)} + \frac{1}{2}O_{2(g)} \quad (5)$$

$$Fe_2(SO_4)_{3(s)} \rightarrow^{\Delta} Fe_2O_{3(s)} + 3SO_{2(g)} + \frac{3}{2}O_{2(g)} \quad (6)$$

$$SO_{2(g)} + \frac{1}{2}O_{2(g)} \rightarrow SO_{3(g)} \quad (7)$$

4.4 REO Extraction

Sulfated samples of the three different lithotypes were submitted to temperatures ranging from 200 to 800 °C and leached in water under controlled pH. The REO extraction was calculated for each sample. It is defined as the ratio between the amount of remaining REO in the filter cake after water leaching and the initial amount contained in the sample. The results are shown in Fig. 7. Maximum REO extraction was attained at about 700 °C, which varied from 73 to 82%, depending on the sample (Fig. 7a). Acid addition ratios were 0.25, 0.21, and 0.34 kg of sulfuric acid per kilogram of ore, for foscorite, bebedourite, and flogopitite, respectively. The acid addition was a function of the sample composition in which elements from the alkaline and alkaline earth groups are the main acid consumers, followed by phosphor, iron, and aluminum. A sharp drop in REO extraction can be noticed for temperatures higher than 700 °C, reaching extractions close to 0% at 800 °C. This result is unexpected, since the decomposition of lanthanum sulfate (responsible for 24% of total rare earth oxides), is expected to take place at 1100 °C, according to TGA results. The iron and thorium extraction (Fig. 7b) fell drastically at 700 °C, reaching values of lower than 1%. This behavior agrees with TGA results and thermodynamic simulation. The low thorium extraction may be attributed to the atmosphere inside the sample, which may have affected its decomposition in the same way as it affected the rare earth decomposition at temperatures higher than 700 °C. This

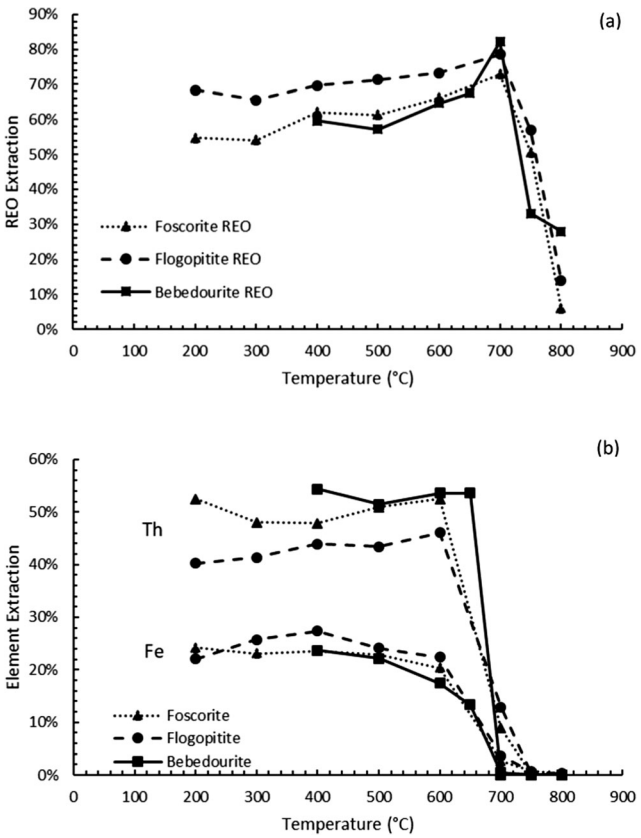

Fig. 7 **a** Rare earths, and **b** iron and thorium extraction obtained for three different lithotypes. Sulfuric acid addition of 0.25, 0.21, and 0.34 kg/kg of ore for foscorite, bebedourite and flogopitite, respectively. Mixing time of 15 min

drastic decrease in Th extraction takes place at temperatures 50 °C lower than that for REE, creating a window for selective extraction for rare earth. If the ore is heated at 700 °C, it is expected to attain a maximum REO extraction and a lower Th and Fe extraction. This scenario is favorable for downstream processing, because iron should be extracted before REE separation by solvent extraction. Thorium, in particular, will follow REE in the downstream process, and even if it is further removed, it may cause disposal problems due to its radioactive nature. The decomposition behavior for some hydrated heavy rare earth sulfates (Dy, Y, Pr, and Sm) shown in Fig. 5 (300–500 °C) was not confirmed by the experimental data, since the ratio LREE/HREE was kept the same after roasting at 700 °C and water leaching. This decomposition behavior agrees with that reported by Nathans and Wendlandt [23].

Other reactions, apart from Eqs. (1)–(7), may be taking place during heating. Equations (8) and (9) are examples of the reverse reaction for sulfation and may take place at temperatures higher than 400 °C where sulfuric acid has already decomposed into gaseous SO_3 and H_2O. The formation of insoluble phosphates or the presence of a reductive atmosphere inside the ore charge may be responsible for the decrease in rare earth extraction at temperatures higher than 750 °C, and the decrease in thorium extraction at temperatures higher than 700 °C. These mechanisms are under investigation and the results will be discussed in future works.

$$REE_2(SO_4)_{3(s)} + 2H_3PO_{4(l)} \rightarrow^{\Delta} 2REEPO_{4(s)} + 3H_2O_{(g)} + 3SO_{3(g)} \quad (8)$$

$$REE_2(SO_4)_{3(s)} + P_2O_{5(g)} \rightarrow 2REEPO_{4(s)} + 3SO_{3(g)} \quad (9)$$

The increase in REO extraction at 700 °C may be due to structural changes taking place in the crandallite structure [27], a mineral which hosts some of the REE present in the ore.

5 Conclusions

The behavior of rare earth, thorium, and iron during selective extraction of rare earth ores was discussed. Our findings indicated that rare earth-bearing monazite ores may be selectively treated to separate iron and thorium from rare earth elements if submitted to sulfation, roasting at 700 °C, and water leaching under controlled pH. This process promotes high rare earth extraction (between 70 and 80%), low iron, and thorium extraction (below 1%) with low acid consumption (between 0.21 and 0.34 kg of acid for 1 kg of ore). There was very good agreement for sulfate decomposition between thermodynamic simulation and TGA results for iron and lanthanum sulfates. The results also show that lanthanum sulfate decomposes in a two-step process, likely forming $La_2O_2SO_4$ as an intermediate compound, which could not be predicted from thermodynamic evaluation. The key stage for selective extraction is roasting, in which iron sulfate decomposes into iron oxide and releases SO_3 gas. The iron sulfate decomposition is achieved at 700 °C, a condition in which rare earths achieve maximum extraction. The amount of insoluble rare earth compounds increases sharply at temperatures higher than 750 °C, decreasing the amount of recoverable rare earth elements during the leaching step and therefore rendering the processes ineffective for rare earth extraction. This temperature is lower than expected for sulfate decomposition into oxides and may be related to the formation of phosphate compounds.

Acknowledgments The authors would like to thank Vale S.A., especially Cassia Souza, Keila Gonçalves and Patrice Mazzoni for sample, material support, and the permission for publishing the results of this investigation. The authors are also thankful to Wagner Soares, Luzia Chaves, and Vale—CDM technicians, for their support in this work. V Ciminelli and D Majuste acknowledge the support from CNPq—*Conselho Nacional de Desenvolvimento Científico e Tecnológico*, CAPES—*Coordenação de Aperfeiçoamento de Pessoal de Nível Superior*—Brasil—Finance Code 001, and FAPEMIG—*Fundação de Amparo à Pesquisa de Minas Gerais*.

Compliance with Ethical Standards

Conflict of Interest The authors declare that they have no conflict of interest.

References

1. Lucas J, Lucas P, Le Mercier T, Rollat A, Davenport WGI (2014) Rare earth: science, technology, production and use, 1st edn. Elsevier, Amsterdam
2. Lehmann B (2014) Economic geology of rare earth elements in 2014: a global perspective. European Geologist 37:21–24
3. Gupta CK, Krishnamurthy N (2005) Extractive metallurgy of rare earths. CRC Press, Boca Raton
4. U.S Geological Survey (2016) Mineral commodity summary, Reston, Virginia, USA
5. SNL/S&P Global, Historical prices (2017) www.snl.com. Accessed 8 July 2018
6. Pradip, Fuerstenau DW (1991) The role of inorganic and organic reagents in the flotation separation of rare-earth ores. Int J Miner Process 32:1–22
7. Zhang J, Zhao B, Schereiner B (2016) Separation hydrometallurgy of rare earth elements. Springer, Basel
8. Merritt RR (1990) High temperature methods for processing monazite: reaction with calcium chloride and calcium carbonate. J Less-Common Met 166:197–210
9. Renou A, Tognet J (2003) Procede de traitement d'un minerai de terres rares a teneur elevee en fer, FR2 826 667 – A1, France
10. Huang X, Li H, Long Z, Liu Y, Zhao N, Zhang G (2009) A process of smelting monazite rare earth ore Rich in Fe, WO2009/021389
11. Mackowski SJ, Raiter R, Soldenhoff KH, Ho EM (2009) Recovery of rare earth elements, US2009/0272230 A1
12. Boudreault R, Primeau D, Fournier J, Simoneau R, Garcia MC, Krivanec H, Dittrich C (2012) Process for recovering rare earth elements from various ores, EP 3141621A1

13. Berni TV, Pereira AC, Mendes FD, Tude AL (2013) System and method for rare earth extraction. Patent US 2013/0336856 A1
14. Teixeira LAV, Silva RG (2015) System and process for selective rare earth extraction with sulphur recovery. Patent US 2015/0329940 A1
15. Onal MAR, Borra CR, Guo M, Blanpain B (2015) Recycling of NdFeB magnets using sulfation, selective roasting and water leaching. J Sustain Metall 1:199–215
16. Verbaan N, Bradley K, Brown J, Mackie S (2015) A review of hydrometallurgical flowsheets considered in current REE projects, In: Simandl GJ, Neetz M (eds) Symposium on strategic and critical materials proceedings. British Columbia Ministry of Energy and Mines, British Columbia Geological Survey Paper 2015-3, Victoria, British Columbia, pp 147–162
17. Testa FG, Avelar AN, Silva RG, Souza CC (2016) Mineralogical characterization and alternative to concentrate the rare earth lithotypes from alcaline complex of Catalão – GO. Associação Brasileira de Metalurgia, Materiais e Mineração, São Paulo. https://doi.org/10.4322/2176-1523.1064
18. HSC Chemistry (2015) Equilibrium calculations. Outotec, Pori
19. Brod JA, Gibson SA, Thompson RN, Junqueira-Brod TC, Seer HJ, Moraes LC, Boaventura GR (2000) Kamafugite affinity of the Tapira alkaline-carbonatite complex (Minas Gerais, Brazil). Rev Bras Geosci 30:404–408
20. Ribeiro CC (2008) Geology, Geometallurgy, controls and genesis of phosphorus deposits, rare earths and titanium of the Catalão carbonate complex I, Goias. Dr. Thesis, Universidade de Brasília (*in portuguese*)
21. Bainbridge DW (1973) Sulfation of a nickeferous laterite. Mater Trans 4(7):1655–1658
22. Wendlandt WW, George TD (1961) A differential thermal analysis study of the dehydration of the rare-earth (iii) sulphate hydrates. The heats of dehydration. J Inorg Nucl Chem 19:245–250
23. Nathans MW, Wendlandt WW (1962) The thermal decomposition of the rare-earth sulphates. J Inorg Nucl Chem 24:869–879
24. Lowell PS, Schwitzgebel K, Parsons TB, Sladek KJ (1970) Selection of metals oxides for removing SO_2 from fuel gas. I&DC Research Results Service, ACS, Washington, DC
25. Poston JA Jr, Siriwardane RV, Fisher EP, Miltz AL (2003) Thermal decomposition of the rare earth sulfates of cerium (III), cerium (IV), lanthanum (III) and samarium (III). Appl Surf Sci 214:83–102
26. Hwdwgus AJ, Fukker K (1956) Ver. Gluhlampen-u. Elektrizitats-werke, A.-G., Tungsram, Budapest. Z Anorg Allg Chem 284:20–30
27. Francisco EAB, Prochnow LI, Toledo MCM, Ferrari VC, Jesus SL (2007) Thermal treatment of aluminous phosphates of the crandallite group and its effect on phosphorus solubility. Sci Agric, (Piracicaba, Brazil) 64(3):269–274. https://doi.org/10.1590/S0103-90162007000300009